Electronic Supplementary Material (ESI) for Materials Horizons.
This journal is © The Royal Society of Chemistry 2021

Supporting Information

Balanced Infrared Nonlinear Optical Performance Achieved by Modulating Covalency and Ionicity Distributions in Electron Localization Function Map

Bin-Wen Liu, Xiao-Ming Jiang,* Shao-Min Pei, Wen-Fa Chen, Long-Qi Yang and Guo-Cong Guo*

State Key Laboratory of Structural Chemistry, Fujian Institute of Research on the Structure of Matter, Chinese Academy of Sciences, Fuzhou, Fujian 350002, P. R. China

Table of Contents

1. Experimental Procedures

Syntheses

Polycrystalline samples of $A_2Ba_3Li_6Ga_{28}S_{49}$ (A = K, **1**; Rb, **2**; Cs, **3**) were synthesized via high-temperature solid-state reactions. Raw materials Ba (99.9%, 0.52 mol), Ga (99.99%, 1.58 mol), S (99.99%, 3.67 mol), LiCl (99.9%, 2.53 mol) and KCl (99.9%, 2.04 mol for **1**), RbCl (99.9%, 1.41 mol for **2**), CsCl (99.9%, 1.13 mg for **3**) were load into a quartz tubes and evacuated to 10^{-4} Torr. Then the reagents were slowly heated to 950 °C in 20 h and kept at that temperature for 96 h, finally cooled to 350 °C in 96 h before the furnace was shut down. Colorless polycrystalline powders of **1**−**3** were obtained. Energy dispersive analysis by X-ray (EDX) was performed with an EDX-equipped Hitachi S-3500 SEM spectrometer on several single crystals. It indicated the presence of A/Ba/Ga/S in the ratios of 2.0:3.2:26.7:47.6, 2.0:3.4:29.7:49.6 and 2.0:3.3:29.0:50.6 for **1**−**3**, respectively (Fig. S1), which agree well with their stoichiometric ratios determined from single-crystal XRD. It should be noted that EDX analysis is unable to detect the Li element.

Structural Refinement and Crystal Data

Single crystal X-ray diffraction data were collected using a Rigaku Pilatus CCD diffractometer equipped with graphite-monochromated Mo-*Kα* radiation (λ= 0.71073 Å) at 293 K. All structures were solved by direct methods and refined by full-matrix least-squares methods on F^2 by SHELX-97. The calculations were performed via the Siemens SHELXTL version 5 package of crystallographic software.[1] All the space groups of **1**−**3** were $P6_3cm$ based on the intensity distribution and systematic extinction of the observed structure factors. The assignment of atoms was based on the bonding characteristics, valence balance, and EDX results. The final structures were examined for additional symmetry with ADDSYM/PLATON.[2]The positional parameters before the last refinement cycles were standardized using the program STRUCTURE TIDY.[3] Further details of the crystal structure investigation(s) may be obtained from the Fachinformationszentrum Karlsruhe, 76344 Eggenstein-Leopoldshafen (Germany), on quoting the depository number CCDC-1923320-1923322 for **1**–**3**, respectively. Powder X-ray diffraction (XRD) patterns were collected in the angular range of 2θ = 5–65° with a scan step width of 0.02° on a Rigaku MiniFlex II X-ray diffractometer with Cu-Kα radiation (λ = 1.54057 Å).

Infrared and UV−Vis−NIR Diffuse Reflectance Spectroscopy

The optical diffuse reflectance spectra of **1**−**3** were measured in the range 2500-250 nm by using a Perkin-Elmer Lambda 900 UV−Vis spectrophotometer. The absorption spectra were calculated from the reflection spectra via the Kubelka−Munk formula: $\alpha/S = (1 - R)^2/(2R)$, where α is the absorption coefficient, S is the scattering coefficient, and R is the reflectance.[4] IR spectra were recorded in the range 4000−400 cm^{-1} by using a Nicolet Magana 750 FT−IR spectrophotometer.

Second Harmonic Generation (SHG) Measurements

The SHG measurements of **1**−**3** were investigated by modified Kurtz-Perry powder technique [5] using a 1910 nm laser beam. Both microcrystalline samples of both **1**−**3** and benchmark AGS were sieved into several distinct particle

sizes ranges (30−50, 50−75, 75−100, 100−150, and 150−200 μm) for the phase-matching measurements. The SHG signals were detected by using a charge-coupled device.

Laser-induced Damaged Threshold (LIDT) Measurements

The LIDTs were evaluated on polycrystalline samples by the single pulse measurement method,[6] using a high-power 1064 nm laser irradiation with pulse width τ_p of 10 ns. Microcrystalline phases **1−3** and benchmark AGS in the same particle size (150−200 μm) were prepared for the test. The measurement processes were performed by gradually increasing the laser power until the color of the irradiated spots on the sample changed, at which the laser power and areas of the damage spots were marked to estimate the value of LIDT. The wide band gaps of **1−3** is one main reason that results in their low dielectric damage and much high LIDT. In addition, the thermal expansion coefficient (TEC) and thermal expansion anisotropy (TEA) can strongly influence thermal damage and LIDT. NLO materials with smaller TEC and TEA tend to sustain greater thermal shock under laser irradiation and to exhibit larger LIDT. The lattice parameters of **1−3** and reference AGS were measured as a function of temperature using a single-crystal X-ray diffractometer from 100-400 K with a step of 20 K. Plots of thermal expansion of the *a* (or *b*) and *c* axes are shown in Figure S5. The calculated TEC (α_a and α_c) and TEA (δ) defined as $\delta = \max\{(\alpha_i-\alpha_j)/\alpha_{i\ (i,\ j\ =\ a,\ c)}\}$ were shown in Table S5. The TEAs of **1−3** are 0.38, 0.55 and 0.44, respectively, which are smaller than that of AGS (2.95).[7] These results are consistent with the fact that the LIDTs of **1−3** are much higher than that of AGS.

Electronic Structures

The electronic structure calculations of **1−3** based on density functional theory were performed using the CASTEP package.[8] The generalized gradient approximation [9] was chosen as the exchange-correlation functional, and the norm-conserving pseudopotential [10] was used. The plane-wave cutoff energy was 800 eV for all compounds, and the threshold of 10^{-5} eV was set for the self-consistent field convergence of the total electronic energy. The orbital electrons of K-$3s^23p^64s^1$, Rb-$4s^24p^65s^1$, Cs-$5s^25p^66s^1$, Ba-$5s^25p^66s^2$, Ga-$3d^{10}4s^24p^1$, S-$3s^23p^4$ and Li-$2s^1$ were treated as valence electrons. The numerical integration of the Brillouin zone was performed using 2 × 2 × 2 Monkhorst–Pack κ-point meshes for three compounds. The Fermi level (E_f =0 eV) was selected as the reference.

linear and nonlinear optical properties: The frequency-dependent SHG susceptibility of **1−3** was calculated based on density functional perturbation theory using the ABINIT computer code package [11] and sum formalism of Sharma, where the SHG susceptibility can be divided into three major contributions: the interband transitions $\chi^{abc}_{inter}(2\omega,\omega,\omega)$, the intraband transitions $\chi^{abc}_{intra}(2\omega,\omega,\omega)$ and the modulation of interband terms by intraband terms $\chi^{abc}_{mod}(2\omega,\omega,\omega)$.[12,13]

$$\chi^{abc}_{inter}(2\omega,\omega,\omega) = \frac{e^3}{\hbar^2\Omega}\sum_{nml}\sum_{k} w_k\left\{\frac{2r^{a}_{nm}\{r^{b}_{ml}r^{c}_{ln}\}}{(\omega_{ln}-\omega_{ml})(\omega_{mn}-2\omega)} - \frac{1}{(\omega_{mn}-\omega)}\left[\frac{r^{c}_{lm}\{r^{a}_{mn}r^{b}_{nl}\}}{(\omega_{nl}-\omega_{mn})} - \frac{r^{b}_{nl}\{r^{c}_{lm}r^{a}_{mn}\}}{(\omega_{lm}-\omega_{mn})}\right]\right\}$$

$$\chi^{abc}_{intra}(2\omega,\omega,\omega) = \frac{e^3}{\hbar^2\Omega}\sum_{k} w_k\left\{\sum_{nml}\frac{1}{\omega^2_{mn}(\omega_{mn}-\omega)}\left[\omega_{ln}r^{b}_{nl}\{r^{c}_{lm}r^{a}_{mn}\} - \omega_{ml}r^{c}_{lm}\{r^{a}_{mn}r^{b}_{nl}\}\right] - 8i\sum_{nm}\frac{1}{\omega^2_{mn}(\omega_{n}\right.$$

$$\chi^{abc}_{mod}(2\omega,\omega,\omega) = \frac{e^3}{2\hbar^2\Omega}\sum_{k} w_k\left\{\sum_{nml}\frac{1}{\omega^2_{mn}(\omega_{mn}-\omega)}\left[\omega_{nl}r^{a}_{lm}\{r^{b}_{mn}r^{c}_{nl}\} - \omega_{lm}r^{a}_{nl}\{r^{b}_{lm}r^{c}_{mn}\}\right] - i\sum_{nm}\frac{r^{a}_{nm}\{r^{b}_{mn}\Delta^{c}_{mn}\}}{\omega^2_{mn}(\omega_{mn}-\omega)}\right\}$$

where w_k is the weight of the *k* point, *n*, *m*, and *l* denote the valence states, the conduction states and all states, respectively, with the condition of *l*≠*m*, *n*

The SHG signal intensities of **1**–**3** and AGS measured by modified Kurtz-Perry powder technique were evaluated by the angular average SHG susceptibility tensor square $\langle d_{ijk}^2 \rangle$:[5]

$$\langle d^2 \rangle = \frac{19}{105}\sum_i d_{iii}^2 + \frac{13}{105}\sum_{i\neq j} d_{iii}d_{ijj} + \frac{44}{105}\sum_{i\neq j} d_{iij}^2 + \frac{13}{105}\sum_{ijk,cyclic} d_{iij}d_{jkk} + \frac{5}{7}d_{ijk}^2$$

Compounds **1**–**3** belong to point group of *6mm* and AGS belongs to *-42m*, their $\langle d_{ijk}^2 \rangle$ *are*:

$$\langle d^2 \rangle(1-3) = \frac{19}{105}d_{333}^2 + \frac{26}{105}d_{333}d_{311} + \frac{38}{35}d_{113}^2$$

$$\langle d^2 \rangle(AGS) = \frac{5}{7}d_{123}^2$$

Electron localization function (ELF): ELFs of typical IR and UV/Vis NLO crystals and **1**−**3** were calculated based on B. Sllvl & A. Savin's definitions:[14]

$$ELF = \frac{1}{1 + (\frac{D}{D_h})^2}$$

with

$$D = \frac{1}{2}\sum_i |\nabla\varphi_i|^2 - \frac{1|\nabla\rho|^2}{8\ \ \rho};\ D_h = \frac{3}{10}(3\pi^2)^{5/3}\rho^{5/3}$$

DFT calculations of ELF employed the projector augmented wave method encoded in the Vienna *ab initio* simulation package,[15] the local density approximation (LDA), and the plane wave cutoff energy of 500 eV.

Fractal dimension (FD): FD at isosurface of constant value *x* was calculated based on the definitions:[16]

$$FD(ELF = x) = \lim_{\varepsilon\to 0}\frac{logN(x,\varepsilon)}{log(1/\varepsilon)}$$

where ε is the characteristic length of a box covering the manifold under consideration and given by the cube root of the reciprocal of the total number of pairs of grid points examined. $N(x, \varepsilon)$ is the number of boxes a desired value *x* was present in.

Variable-ELF of FD were calculated using a home-made program based on a line-counting algorithm.[17] 100 ELF levels between 0 and 1 were chosen for the calculation. First check whether the iso-surface for each of *n* chosen points in ELF intersects the line defined by consecutive pairs of points ELF(*i*, *j*, *k*) and ELF(*i*+1, *j*, *k*) in the grid file. Each time n_i satisfies the condition that ELF lies between ELF(*i*, *j*, *k*) and ELF(*i*+1, *j*, *k*), the count in the bin for n_i is incremented by one. This line counting along all $n_y \times n_z$ lines in the *x* direction is then repeated for all $n_x \times n_z$ lines in the *y* direction and all $n_x \times n_y$ lines in the *z* direction.

2. Figures and Tables

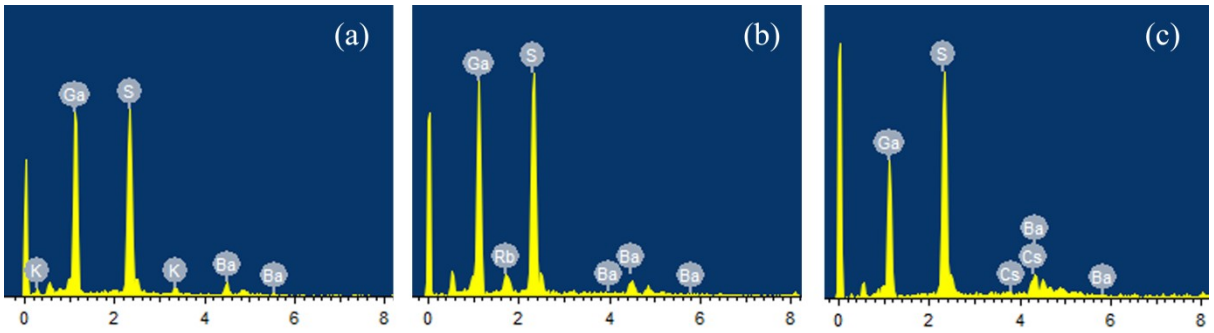

Fig. S1 EDX spectra of **1**(a), **2**(b) and **3**(c).

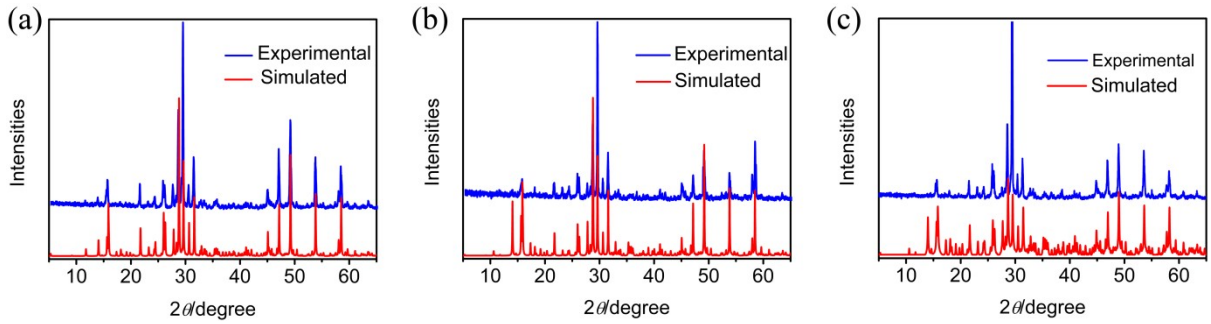

Fig. S2 Experimental and simulated powder X-ray diffraction patterns of **1**(a), **2**(b) and **3** (c).

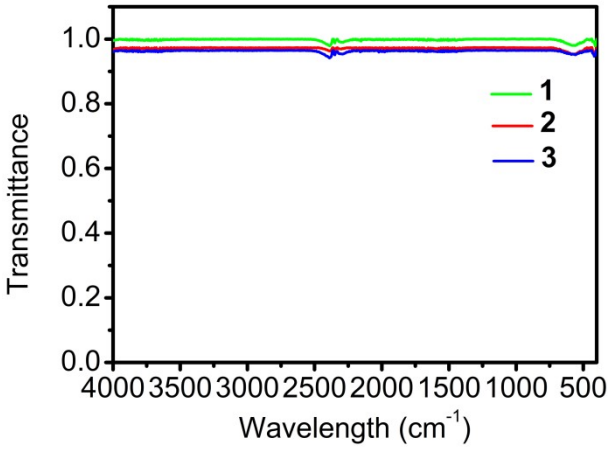

Fig. S3 IR spectra of **1**−**3**.

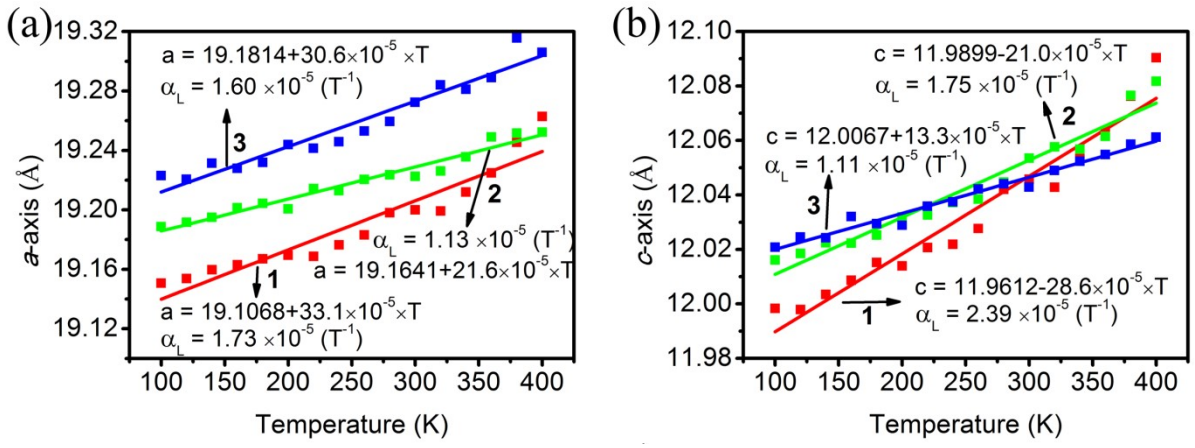

Fig. S4 Temperature variation of the lattice parameters of **1**–**3** (a and b) revealing anisotropic thermal expansion.

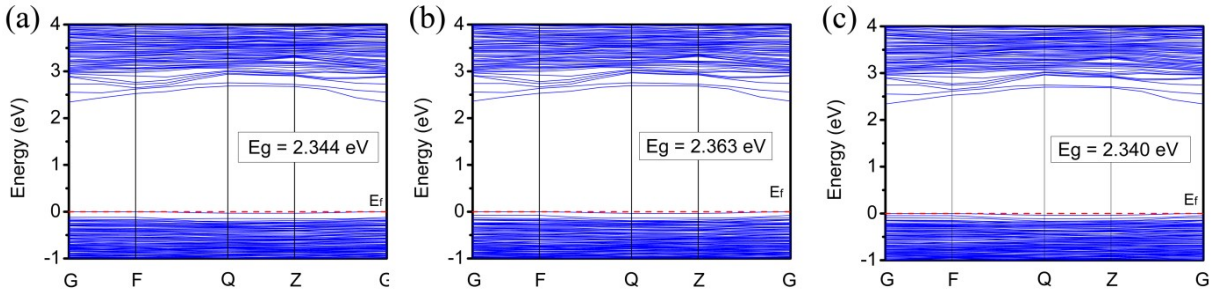

Fig. S5 Calculated electronic band structures of **1**(a), **2**(b) and **3**(c).

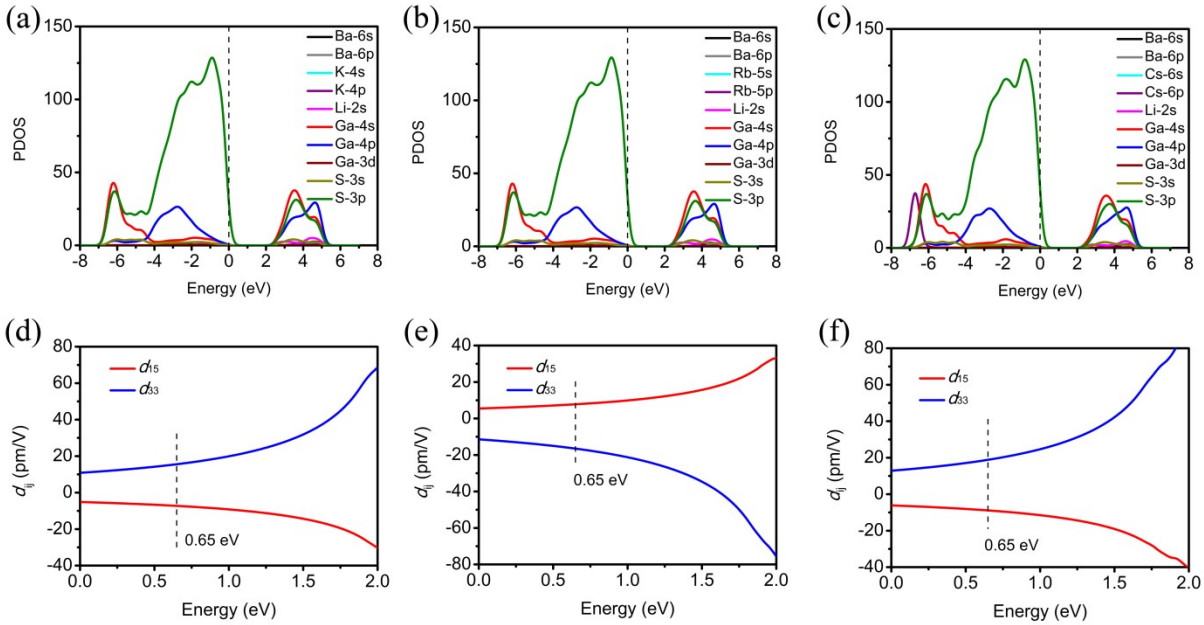

Fig S6 Partial density of states of **1**(a), **2**(b) and **3**(c), and calculated frequency-dependent SHG coefficient tensors of **1**(d), **2**(e) and **3**(f).

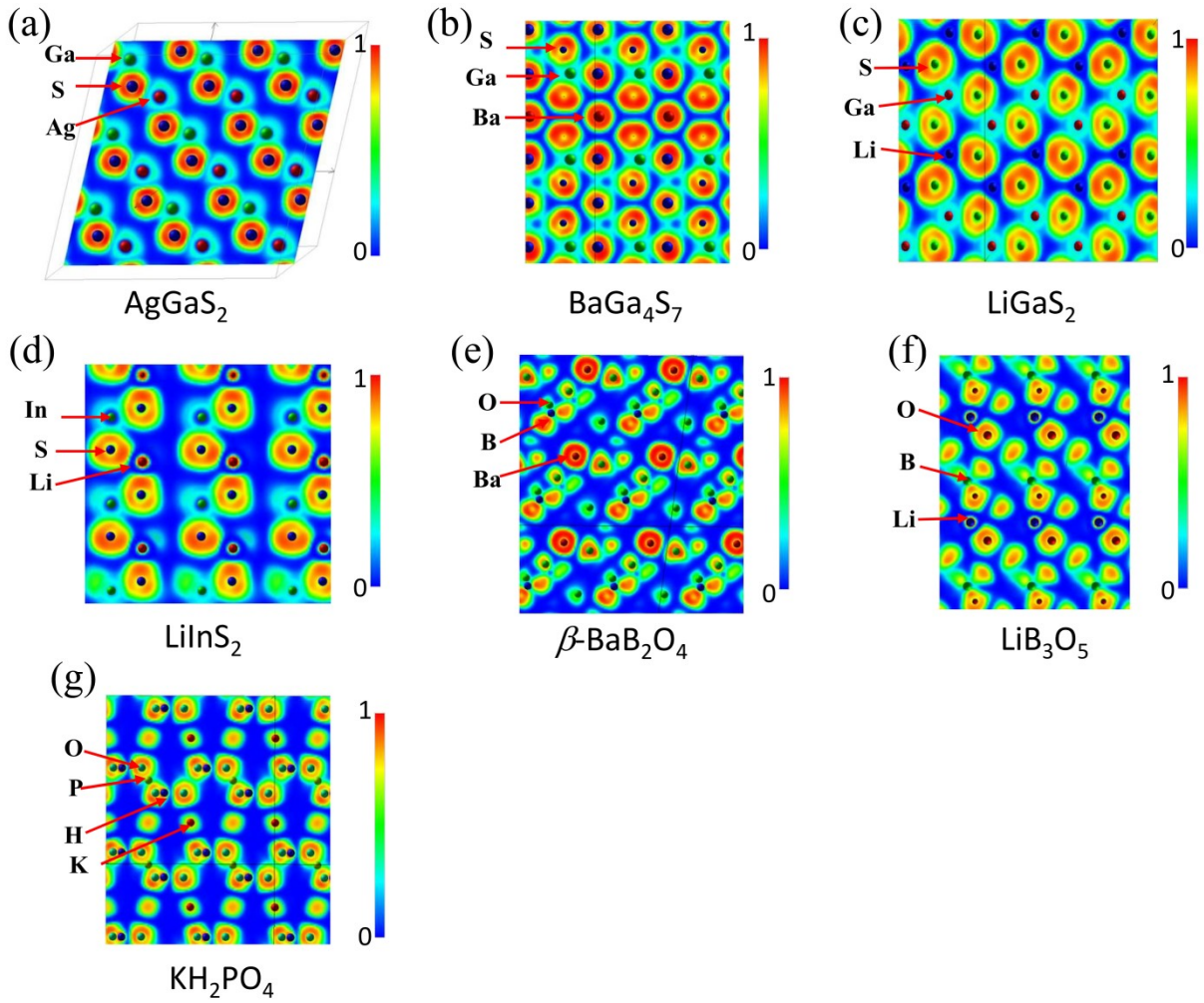

Fig. S7 ELF maps of AGS (a), BGS (B), LGS (c), LIS (d), BBO (d), LBO (e), and KDP (g).

Table S1. Crystallographic data and structure refinement parameters for **1**–**3**.

Empirical formula	$K_2Ba_3Li_6Ga_{28}S_{49}$ (**1**)	$Rb_2Ba_3Li_6Ga_{28}S_{49}$ (**2**)	$Cs_2Ba_3Li_6Ga_{28}S_{49}$ (**3**)
Fw	4054.96	4147.70	4242.58
Space group	$P6_3cm$	$P6_3cm$	$P6_3cm$
a (Å)	19.2135(3)	19.2355(4)	19.3060(4)
c (Å)	12.0481(2)	12.0475(4)	12.0861(4)
V (Å^3)	3851.78(11)	3860.42(17)	3901.23(17)
Z	2	2	2
D_{calcd} (g·cm^{-3})	3.496	3.568	3.612
μ (mm^{-1})	12.562	13.679	13.216
GOF on F^2	1.057	1.016	1.036
$R_1{}^a$ ($I > 2\sigma(I)$)	0.0161	0.0180	0.0239
$wR_2{}^b$ ($I > 2\sigma(I)$)	0.0333	0.0426	0.0546
$R_1{}^a$ (all data)	0.0178	0.0206	0.0275
$wR_2{}^b$ (all data)	0.0337	0.0435	0.0559
Flack x	-0.008(8)	0.006(10)	0.004(13)
$\Delta\rho_{max}/\Delta\rho_{min,}$ (e/Å^{-3})	0.628/−0.659	1.352/−0.762	3.022/-0.797

$^aR = \Sigma||F_o|-|F_c||/\Sigma|F_o|$, $^bwR = (\Sigma(w(F_o{}^2-F_c{}^2)^2)/\Sigma(w(F_o{}^2)^2))^{1/2}$.

Table S2. Atomic fractional coordinates, equivalent isotropic displacement parameters (Å^2) and site occupation for **1**−**3**.

Atoms	x	y	z	U(eq)	SOF
		$K_2Ba_3Li_6Ga_{28}S_{48}$ (**1**)			
K(1)	0.2146(1)	0	0.7600(1)	0.020(1)	0.3333
Ba(1)	0.2146(1)	0	0.7600(1)	0.020(1)	0.6667
K(2)	0.3333	0.6667	0.0151(1)	0.020(1)	0.5
Ba(2)	0.3333	0.6667	0.0151(1)	0.020(1)	0.5
Li(1)	0.4433(3)	0	0.0721(7)	0(1)	1
Li(2B)	0.2343(9)	0	0.3760(18)	0.034(5)	0.5
Li(2)	0.3162(7)	0	0.3296(14)	0.015(3)	0.5
Ga(1)	0.3362(1)	0.4444(1)	0.0694(1)	0.009(1)	1
Ga(2)	0.1172(1)	0	0.0697(1)	0.010(1)	1
Ga(3)	0.1087(1)	0.3262(1)	0.0692(1)	0.009(1)	1
Ga(4)	0.2194(1)	0.4465(1)	0.3120(1)	0.010(1)	1
Ga(5)	0	0	0.2983(1)	0.009(1)	1
Ga(6)	0.1122(1)	0.5492(1)	0.3240(1)	0.010(1)	1
S(1)	0.4378(1)	0	0.2658(1)	0.012(1)	1
S(2)	0.2288(1)	0.5620(1)	0.2630(1)	0.014(1)	1
S(3)	0.1127(1)	0	0.2565(1)	0.025(1)	1
S(4)	0.1217(1)	0.3251(1)	0.2561(1)	0.012(1)	1
S(5)	0.3359(1)	0.4459(1)	0.2633(1)	0.009(1)	1
S(6)	0.3244(1)	0	0.5301(1)	0.012(1)	1
S(7)	0.2209(1)	0.4438(1)	0.0068(1)	0.008(1)	1
S(8)	0.6737(1)	0	0.4957(1)	0.011(1)	1
S(9)	0.1228(1)	0.5607(1)	0.0122(1)	0.011(1)	1
S(10)	0	0	-0.0004(2)	0.007(1)	1
S(11)	0.1135(1)	0.2189(1)	0.0016(1)	0.019(1)	1
		$Rb_2Ba_3Li_6Ga_{28}S_{48}$ (**2**)			

Rb(1)	0.7854(1)	1.0000	0.2401(1)	0.024(1)	0.3333
Ba(1)	0.7854(1)	1.0000	0.2401(1)	0.024(1)	0.6667
Rb(2)	0.6667	0.3333	0.9853(1)	0.029(1)	0.5
Ba(2)	0.6667	0.3333	0.9853(1)	0.029(1)	0.5
Li(1)	0.5567(4)	1.0000	0.9287(10)	0(2)	1
Li(2B)	0.7672(12)	1.0000	0.6230(20)	0.022(6)	0.5
Li(2)	0.6825(11)	1.0000	0.6750(20)	0.023(5)	0.5
Ga(1)	0.6638(1)	0.5556(1)	0.9308(1)	0.008(1)	1
Ga(2)	0.8827(1)	1.0000	0.9296(1)	0.009(1)	1
Ga(3)	0.8912(1)	0.6739(1)	0.9308(1)	0.009(1)	1
Ga(4)	0.7809(1)	0.5535(1)	0.6879(1)	0.008(1)	1
Ga(5)	1.0000	1.0000	0.7014(1)	0.009(1)	1
Ga(6)	0.8875(1)	0.4504(1)	0.6762(1)	0.009(1)	1
S(1)	0.5611(1)	1.0000	0.7356(2)	0.013(1)	1
S(2)	0.7718(1)	0.4385(1)	0.7376(1)	0.014(1)	1
S(3)	0.8873(1)	1.0000	0.7427(2)	0.021(1)	1
S(4)	0.8790(1)	0.6745(1)	0.7437(1)	0.012(1)	1
S(5)	0.6645(1)	0.5541(1)	0.7373(1)	0.008(1)	1
S(6)	0.6754(1)	1.0000	0.4708(1)	0.011(1)	1
S(7)	0.7792(1)	0.5567(1)	0.9934(1)	0.008(1)	1
S(8)	0.3262(1)	1.0000	0.5040(1)	0.011(1)	1
S(9)	0.8781(1)	0.4397(1)	0.9878(1)	0.011(1)	1
S(10)	1.0000	1.0000	1.0000(2)	0.006(1)	1
S(11)	0.8867(1)	0.7812(1)	0.9978(1)	0.017(1)	1
		$Cs_2Ba_3Li_6Ga_{28}S_{48}$ (**3**)			
Cs(1)	0.2146(1)	0	0.7600(1)	0.020(1)	0.3333
Ba(1)	0.2146(1)	0	0.7600(1)	0.020(1)	0.6667
Cs(2)	0.3333	0.6667	0.0151(1)	0.020(1)	0.5
Ba(2)	0.3333	0.6667	0.0151(1)	0.020(1)	0.5
Li(1)	0.4441(5)	0	0.0718(14)	0(2)	1
Li(2B)	0.2318(16)	0	0.3840(30)	0.026(8)	0.5
Li(2)	0.3199(15)	0	0.3240(30)	0.019(6)	0.5
Ga(1)	0.3361(1)	0.4441(1)	0.0692(1)	0.009(1)	1
Ga(2)	0.1171(1)	0	0.0709(1)	0.009(1)	1
Ga(3)	0.1088(1)	0.3259(1)	0.0694(1)	0.009(1)	1
Ga(4)	0.2187(1)	0.4462(1)	0.3121(1)	0.009(1)	1
Ga(5)	0	0	0.2989(1)	0.009(1)	1
Ga(6)	0.1124(1)	0.5497(1)	0.3234(1)	0.010(1)	1
S(1)	0.4399(1)	0	0.2635(2)	0.014(1)	1
S(2)	0.2268(1)	0.5603(1)	0.2617(2)	0.014(1)	1
S(3)	0.1126(1)	0	0.2573(2)	0.021(1)	1
S(4)	0.1203(1)	0.3257(1)	0.2561(2)	0.014(1)	1
S(5)	0.3353(1)	0.4463(1)	0.2623(2)	0.008(1)	1
S(6)	0.3249(1)	0	0.5285(2)	0.014(1)	1
S(7)	0.2205(1)	0.4423(1)	0.0063(1)	0.008(1)	1
S(8)	0.6740(1)	0	0.4969(2)	0.012(1)	1
S(9)	0.1202(1)	0.5598(1)	0.0117(1)	0.012(1)	1
S(10)	0	0	0.0005(3)	0.006(1)	1
S(11)	0.1132(1)	0.2185(1)	0.0029(2)	0.017(1)	1

Table S3. Powder laser-induced damage thresholds (LIDTs) of **1**−**3** and reference AGS.

Compounds	Damage energy (mJ)	Spot area (cm^2)	τ_p (ns)	Damage threshold [$MW \cdot cm^{-2}$]
1	36.0	0.05	10	72.0
2	34.5	0.05	10	69.0
3	33.4	0.05	10	66.8
AGS	2.0	0.05	10	4.0

Table S4. Thermal expansion coefficients α_L of **1**−**3** and reference AGS along the *a*, *b*, and *c* directions, and their thermal expansion anisotropy (δ) defined as $\delta = \max\{(\alpha_i-\alpha_j)/\alpha_{i\,(i,j=a,c)}\}$.

	α_L ($\times 10^{-5}$ K^{-1})			
	1	**2**	**3**	AGS
a=*b*	1.73	1.13	1.60	2.09
c	2.39	1.75	1.11	-1.07
δ	0.38	0.55	0.44	2.95

Table S5. Calculated ELF FD peak height and typical experimental d_{ij} of well-known IR NLO crystals in Figure 4c. The d_{ij} values for IR and UV/Vis NLO crystals are those measured at wavelengths close to 2.0 μm and 1.064 μm, respectively. For each crystal, the selected d_{ij} is the largest one among all non-vanishing tensors.

Crystal	FD peak height	d_{ij} (pm/V)
IR NLO crystals		
AGS	0.08	d_{36}=13.7[18]
LGS	0.021	d_{31} = 5.8 [19]
LIS	0.034	d_{31} = 7.7 [20]
BGS	0.02	d_{32} = 5.7 [21]
UV/Vis NLO crystals		
BBO	0.009	d_{22} = 2.2 [22]
LBO	0.005	d_{32} = 0.85 [23]
KDP	0.001	d_{36} = 0.39 [24]

Table S6. Calculated and typical experimental band gap and LIDT of well-known IR NLO crystals in Figure 4d. The LIDT values are those measured at wavelength, repetition frequency and pulse width close to 1.064 μm, 10 Hz and 10 ns respectively for all crystals. For convenience, the LIDTs are scaled by 5*$LIDT^{1/4}$.

Crystal	FD average	band gap (eV)	LIDT (GW/cm^2)
AGS	2.189	2.7 [25]	0.03 [26]
LGS	2.287	4.15 [27]	0.24 [19]

LIS	2.279	3.56 [28]	0.10 [29]
BGS	2.230	3.54 [30]	0.08 [30]
BBO	2.334	6.43 [31]	4.5 [32]
LBO	2.332	7.75 [33]	8.0 [34]
KDP	2.307	6.95 [35]	6.4 [36]

3. References

1. Siemens, SHELXTL Version 5 Reference Manual; Siemens Energy &Automation Inc.: Madison, WI, 1994.

2. A. L. Spek, PLATON, A Multipurpose Crystallographic Tool; Utrecht University, Utrecht, The Netherlands, 2005.

3. L. M. Gelato and E. Parthé, *J. Appl. Crystallogr*. 1987, **20**, 139−143.

4. G. Korum, Reflectance Spectroscopy, Springer, New York, 1969.

5. S. K. Kurtz and T. T. Perry, *J. Appl. Phys*., 1968, **39**, 3798−3813.

6. M.-J. Zhang, X.-M. Jiang, L.-J. Zhou and G.-C. Guo, *J. Mater. Chem. C,* 2013, **1**, 4754−4760.

7. B.-W. Liu, H.-Y. Zeng, X.-M. Jiang and G.-C. Guo, *CCS Chemistry,* 2020**, 2**, 964-973.

8. (a) M. C. Payne, M. P. Teter, D. C. Allan, T. A. Arias and J. D. Joannopoulos, *Rev. Mod. Phys*., 1992, **64**, 1045−1097. (b) S. J. Clark, M. D. Segall, C. J. Pickard, P. J. Hasnip, M. J. Probert, K. Refson and M. C. Z. Payne, *Z. Kristallogr. Cryst. Mater*., 2005, **220**, 567−570.

9. J. P. Perdew, J. A. Chevary, S. H. Vosko, K. A. Jackson, M. R. Pederson, D. J. Singh and C. Fiolhais, *Phys. Rev. B*., 1992, **4***6*, 6671−6687.

10. D. R. Hamann, M. Schlüter, C. Chiang, *Phys. Rev. Lett*., 1979, **43**, 1494−1497.

11. (a) X. Gonze, *Phys. Rev. A*, 1995, **52**, 1086−1095; (b) X. Gonze, *Phys. Rev. A*, 1995, *52*, 1096−1114; (c) X. Gonze, *Phys. Rev. B*, 1997, *55*, 10337−10354; (d) X. Gonze and C. Lee, *Phys. Rev. B*, 1997, **55**, 10355−10368.

12. S. Sharma and C. Ambrosch Draxl, *Phys. Scripta*., 2004, **T109**, 128−134.

13. S. Sharma, J. K. Dewhurst and C. Ambrosch-Draxl, *Phys. Rev. B,* 2003, **67**, 165332.

14. B. Silvi and A. Savin, *Nature*, 1994, **371**, 683−686.

15. (a) G. Kresse and J. Hafner, *Phys. Rev. B*, 1993, **47**, 558−561; (b) G. Kresse and J. Hafner, *Phys. Rev. B*, 1994, **49**, 14251−14269; (c) G. Kresse and J. Furthmüller, *Comput. Mat. Sci*., 1996, **6**, 15−50; (d) G. Kresse and J. Furthmüller, *Phys. Rev. B*, 1996, **54**, 11169−11186.

16. I. N. Bronshtein, K. A. Semendyayev, G. Musiol and H. Muehlig, *Handbook of Mathematics*, Springer, 2003.

17. K. Meindl and J. Henn, *Acta Cryst.,* 2008, **A64**, 404–418.

18. J. J. Zondy, D. Touahri and O. Acef, *J. Opt. Soc. Am. B,* 1997, **14**, 2481−2497.

19. L. Isaenko, I. Vasilyeva, A. Merkulov, A. Yelisseyev and S. Lobanov, *J Crystal Growth*, 2005, **275**, 217−223.

20. L. Isaenko, A. Yelisseyev, S. Lobanov, V. Petrov, F. Rotermund, J. J. Zondy, G. H. M. Knippels, Mater. Sci. Semicond. Processing, 2001, **4**, 665−668.

21. Y. F. Guo, Y. Q. Zhou, X. S. Lin, W. D. Chen, N.Ye, *Opt. Mater*., 2014, **36**, 2007−2001.

22. I. Shoij, H. Nakamura, K, Ohdaira, T. Kondo, R. Ito, T. Okamoto, K. Tatsuki, S. Kubota, *J. Opt. Soc. Am. B*, 1999, **14**, 620−624.

23. D. A. Roberts, *IEEE J. Quant. Electr*., 1992, **28**, 2057−2074.

24. I. Shoij, T. Kondo, A. Kitamoto, M. Shirane, R. Ito, *J. Opt. Soc. Am. B*, 1997, **14**, 2286−2294.

25. S. Chandra, T. H. Allik, G. Catella, J. A. Hutchinsion, In: Advanced Solid-State Lasers, OSA Trends om Optics and Photonics Series, by W. R, Bosenberg, M. M. Fejer (OSA, Washiongton DC) 1998, **19**, 282−284.

26. Physical-Chemical Properties of Semiconductors. Handbook. (Nauka, Moscow, In Russian, 1997.

27. A. Tyazhev, V. Vedenyapin, G. Marchev, L. Isaenko, D. Kolker, S. Lobanov, V. Petrov, A. Yelisseyev, M. Starikova and J.-J. Zondy, *Optical Mater.*, 2013, **35**, 1612−1615.

28. S. Fossier, S. Salau¨n, J. Mangin and O. Bidault, *J. Opt. Soc. Am. B*, 2004, **21**, 1981−2007.

29. A. Eifler, V. Riede, J. Bruckner, S. Weise, V. Kramer, G. Liplold, W. Schmitz, K. Bente and W. Grill, *Jpn. J. Appl. Phys.*, 2000, **39**.

30. X. Lin, G. Zhang and N. Ye, *Cryst. Growth. Des.*, 2009, **9**, 1186−1189.

31. H. Kouta, *Appl. Opt.,* 1999, **38**, 545−547.

32. R. H. French, J. W. Ling, F. S. Ohuchi and C. T. Chen, *Phys. Rev*., 1991, **44**, 8496−8502.

33. A. Nebel and R. Beigang, *Opt. Lett*., 1991, **16**, 1729−1731

34. B. H. T. Chai, Optical Crystals. In: CRC Handbook of Laser Science and Technology, Supplement 2: Optical Materials, ed. By M. J. Weber (CRC Press, Boca Raton) 1995, 3−65.

35. R. M. Wood, R. T. Taylor and R. L. Rouse, *Opt. Laser Technol*., 1975, **7**, 105−111.

36. P, Liu, W. L. Smith, H, Lotem, J. H. Bechtel, N. Bloembergen and R. S. Adhav, *Phys. Rev*., 1978, **B17**, 4620−4632.